INVESTIGATING THE COUPLING OF HELICOPTER AERODYNAMICS WITH SIMPACK FOR ARTICULATED AND HINGELESS ROTORS

M. Mindt
DLR Institute of Flight Systems,
Lilienthalplatz 7, 38108 Braunschweig,
Germany

S. Surrey
DLR Institute of Aeroelasticity,
Bunsenstraße 10, 37073 Göttingen,
Germany

Abstract

In this paper the results of a tight coupling of rotor aerodynamics with a rotor model built up in the multibody software SIMPACK are presented. The aerodynamics are calculated by S4, which is a simulation tool developed at the Institute of Flight Systems of the German Aerospace Center. In a first step, the coupling approach was verified via cross code comparison for simple load cases such as hover flight for a hingeless blade with a straight elastic axis. The conclusions drawn for the verification methodology will be pointed out in the beginning of this paper. Investigations of a four bladed rotor in trimmed forward flight condition were conducted, leading to the discovery of a drawback in the representation of flexible beam-like structures in SIMPACK for helicopter applications. Additionally, a model of the articulated 7A rotor has been created. With this rotor a high speed flight condition test case was performed in the S1 wind tunnel and the results of the simulations are compared to the test results. In an attempt to eliminate the modeling deficiencies of the one-dimensional beam, a three-dimensional finite element model of the 7A rotor blade has been built at the Institute of Aeroelasticity as well. A comparison of the eigenmodes and eigenfrequencies of the one- and three-dimensional model will be shown. All investigations presented in this paper were carried out in the course of the project Digital-X.

1. NOMENCLATURE

$\mathbf{A}$	state matrix
$\mathbf{B}$	input matrix
C_L, C_X	rotor lift and propulsive force coefficient
C_n, C_m	section normal force and pitching moment coefficient
CFD	computational fluid dynamics
DoF	degree(s) of freedom
EA	axial stiffness, Nm²
EI	bending stiffness, Nm²
F	force, N
FE	finite element
GJ	torsional stiffness, Nm²
$\mathbf{K}$	stiffness matrix
M	Mach number
$\mathbf{M}$	mass matrix
R	rotor radius, m
$\mathbf{R}$	position vector, m
$\mathbf{a}$	translational acceleration, m/s²
$\mathbf{c}$	displacement, m
$\mathbf{q}$	generalized coordinates
r	rotor radial station, m
t	time, s
$\mathbf{u}$	translational deformation, m
$\mathbf{v}$	translational velocity, m/s
$\mathbf{x}$	state vector
y	lag deflection, m
z	flap deflection, m
$\mathbf{z}$	input vector
α_{Ro}	rotor shaft angle, deg
β	flap angle, deg
ζ_p	prelag, deg
ϑ	elastic torsion, deg
$\boldsymbol{\vartheta}$	rotational deformation, rad
θ_0, θ_c, θ_s	collective, lateral and longitudinal cyclic pitch angle, deg
λ	growth constant
Λ	eigenvalue
μ	advance ratio
σ	rotor geometric solidity
$\boldsymbol{\Phi}$	translational shape function, m
Ψ	rotor azimuth, deg
$\boldsymbol{\Psi}$	rotational shape function, rad
ω	natural frequency, rad/s
$\boldsymbol{\omega}$	rotational velocity, rad/s
Ω	rotor rotational velocity, rad/s

Letters in bold indicate vectors and matrices.

2. INTRODUCTION

In recent years, rotor blade designs have become more and more heteromorphic, incorporating swept tips or even blades swept fore and aft like the Airbus Helicopter H160's main rotor blade [1], [2]. The attachment of the blade to the rotor head varies from articulated to bearingless systems. Furthermore, different damping concepts from elastomeric bearings to linear dampers connecting the blade with the rotor head and interblade dampers are in use. All this leads to the demand of more sophisticated tools in the developmental process, where a large number of operating points of the future helicopter have to be investigated to identify possible problems. This task is carried out using so-called comprehensive rotor codes,

which combine the calculation of the complex aerodynamics of a helicopter in forward flight and the structural dynamics of the blades. Widely used codes are for example CAMRAD II [3], HOST [4], RCAS [5], UMARC [6] and AVINOR [7].

Another comprehensive rotor code, designated S4, was developed at the Institute of Flight Systems of the German Aerospace Center (DLR). S4 incorporates semi-empirical, analytical models for the calculation of the aerodynamic coefficients in compressible, unsteady flow with dynamic stall and yawed flow effects. The code was intensively validated using the experimental data of the HART II wind tunnel test campaign [8], for example.

The structural dynamics in S4 have several limitations, on the other hand. An example being that only one rotating rotor with its center point fixed in space can be modeled, which originates in the initial purpose of the rotor code to prepare wind tunnel tests. The dynamics of the elastic blade are represented by a modal synthesis approach. The modes and frequencies of the blade are calculated by a finite element (FE) preprocessor developed in-house based on the formulation of the differential equations of motion by Houbolt and Brooks [9]. This approach does for example not allow for multiple load paths. As a solution to make use of the validated aerodynamic description and overcome the limitations regarding the structural modeling capabilities, the coupling of S4 aerodynamics with the program SIMPACK was identified.

SIMPACK is a commercial multibody tool able to calculate the interaction of rigid bodies undergoing large relative motions. Also, elastic bodies can be included using FE codes like the NASA structural analysis code NASTRAN for preprocessing. With the FE code the mass and stiffness matrix and the mode shapes of the flexible body, as well as the geometric stiffening due to unit loads have to be computed. A SIMPACK preprocessor tool then calculates the data needed for the representation of the flexible body in the multibody environment based on the FE results and saves the data to the so-called flexible body input (fbi) file.

Each body motion is described with respect to the previous body in the kinematic tree within SIMPACK which is also called relative coordinate description. Other MBS programs like ADAMS use an absolute formulation describing the motion of each body in a global coordinate system. The relative description and exploitation of the kinematic tree structure allow for a smaller number of equations to be solved in the solution process; therefore, SIMPACK stands out due to its computational speed.

SIMPACK has been applied in numerous areas, but since the operating conditions of a rotating helicopter blade are a specialized application with complex dynamic effects, the validation of the correct implementation of all dynamic effects arising at the elastic rotor blade has to be given special emphasis.

3. VERIFICATION OF THE COUPLING: HOVER

The coupling concept and its realization was published in [10], including the presentation of a hover trim result. The verification of the coupling chain was done via cross code comparison with S4 as standalone code. Not only because of the limitations of the structural modeling capabilities in S4, but also due to the need of step-by-step verifications of different aspects, simplified elastic body models of the blades were used. In the course of the investigations, some differences in the consideration of dynamic effects in the two tools were found that could not be eliminated by usage of simpler, but still realistic blade models. The approaches used to account for these differences are listed in TAB 1 and will be explained here. A more detailed discussion of the single features can be found in [10].

The first entry is related to the simplifications made in S4. Previously, only the main mode components were used for the modal synthesis in S4. As SIMPACK always uses the complete calculated modes, a simplified implementation to account for the secondary mode components in S4 was implemented. That is, the secondary components of the single modes are added to the deflections resulting from the main components. The effects of the additional deflections are accounted for in the aerodynamics but the dynamic effects in the mass terms are neglected. Another simplification of S4 is that the modes of the blade do not change with the pitch angle, i.e. the mode shapes used are always those of the reference configuration, assuming small variations around it. To avoid a change in the mode shapes in SIMPACK, the blade is also not structurally pitched and only the forces acting on the blade elements are transformed according to the pitch settings. After successful completion of the verification it is planned to rotate the blades according to the pitch setting again to make full use of the capabilities of SIMPACK, however.

In SIMPACK, the inertia terms depend on the deformation of the blade. Therefore, it was believed that also the influence of the deformation on the acting centrifugal loads was accounted for by SIMPACK. The resulting differences were expected to be below two percent in typical helicopter applications and hence no compensation was introduced. New findings on this issue can be found in section 4.2.3.

Topic	SIMPACK	S4	Verification
Mode shapes	Fully coupled	Structurally uncoupled	Coupled motions implemented in S4 (simplified)
Effect of pitch on modes	incorporated	ignored	Fixed structural pitch in SIMPACK
Centrifugal loads in differential equations of motion	Dependent on deformation	Only dependent on RPM	No compensation (deviation <2%)
Propeller moment	Not incorporated in 1D beam model	Simplified using formulation for a flat plate	Additional force-element in SIMPACK

TAB 1 Modeling differences between SIMPACK and S4 and approach for verification [10]

Due to the blade modeling approach as a one-dimensional (1D) beam used in NASTRAN, there is no propeller moment acting in SIMPACK. This effect is quite important for the correct consideration of the torsional dynamics of a rotating blade and therefore had to be added into the SIMPACK model. The implementation was done via force elements in SIMPACK that apply the moments arising for the individual finite elements at the blade.

4. DYNAMIC RESPONSE

Since the verification of the coupling chain was finished for the simplified blade in hover test cases, the next step was to take a look at the dynamic behavior of the rotor apart from mode shapes and eigenfrequencies. For this, a four-bladed rotor using the simplified blade as used in [10] was created in SIMPACK. The model was generated using an automated tool named “Rotor Configurator” that was developed in-house and sets up the complete helicopter model including all entries of the input and output vector needed for the coupling. The input vector consists of the rotor rotational and blade pitch settings as well as the aerodynamic forces acting on the blade elements transferred from S4. The output vector transfers all translational and rotational deflections, velocities and accelerations of the blade elements back to S4. The script was also enhanced by the generation of all elements needed to compute and apply the propeller moment at the blade’s finite elements. In S4, the definition of the coupling interface was extended for multiple blades.

4.1. The Effect of Torsional Inertia

As pointed out in TAB 1, the approach for the verification includes no structural pitching of the blade in SIMPACK. This however neglects the effect of the torsional inertia opposing a change in the pitch angle of the blade. In forward flight, a cyclic change of the blade pitch has to be introduced to account for the asymmetric flow conditions resulting from the vector addition of flight velocity and rotation of the blade. Therefore, the effect of torsional inertia has to be apparent to accurately capture the torsional dynamics of the blade in forward flight condition. This is done in the SIMPACK model by the implementation of an additional force element for each finite element applying the inertial moments on the elastic blade depending on the blade pitch acceleration. The generation of all required elements in the SIMPACK model was included in the “Rotor Configurator”. The effect of torsional inertia due to elastic torsion of the blade is incorporated inherently in the SIMPACK model.

4.2. Coriolis Forces

After the implementation of the additional force elements, the first calculations of the rotor in a fast forward flight condition showed the lack of a higher harmonic component in the lag deflections and less hub vibrations in the SIMPACK calculations compared to S4. This lead to the suspicion that Coriolis forces in lag direction as a result of elastic bending of the blade are not considered in the SIMPACK model.

4.2.1. Origin of the Coriolis force

The so called Coriolis acceleration is acting on a rotating body if this body moves relatively to its axis of rotation. The Coriolis acceleration $\boldsymbol{a_{Co}}$ can be calculated as

$$\boldsymbol{a_{Co}} = 2\,\boldsymbol{\omega}\times\boldsymbol{v}, \tag{1}$$

where $\boldsymbol{\omega}$ is the angular velocity vector, $\boldsymbol{v}$ is the translational velocity vector and all entities are measured in a frame rotating with the body [11]. The Coriolis force is resulting from the body’s inertia, opposing the acceleration. In the case of a rotor blade, Coriolis forces arise when the blade exhibits a flap or lag movement. Flap movement is defined as the motion of the blade perpendicular to the rotor plane, positive upwards, and lag describes the movement in the rotor plane, which is measured positive forwards.

To illustrate this, the simple case of a rigid blade fulfilling a flap movement as depicted in FIG 1 shall be used. It can be seen that as the blade flaps upwards, the mass points of the blade also move towards the axis of rotation by Δr. Thus, an acceleration term in y-direction results from the cross product

$$\boldsymbol{a_{Co}} = 2\begin{Bmatrix}0\\0\\\Omega\end{Bmatrix}\times\begin{Bmatrix}v_x\\0\\v_z\end{Bmatrix}=\begin{Bmatrix}0\\2\Omega v_x\\0\end{Bmatrix}. \tag{2}$$

The resulting acceleration term directly excites the lag motion. Hence, the important part of the flapping motion is the radial movement of the mass caused by the nonlinear path of motion. In the case of a lag movement of the blade, two Coriolis terms are resulting because of the different axis of movement:

$$\boldsymbol{a_{Co}} = 2\begin{Bmatrix}0\\0\\\Omega\end{Bmatrix}\times\begin{Bmatrix}v_x\\v_y\\0\end{Bmatrix}=2\Omega\begin{Bmatrix}-v_y\\v_x\\0\end{Bmatrix}. \tag{3}$$

The radial component in the first line of the vector also indirectly excites the flap motion when a flap angle β is apparent by

$$a_{Flap} = -2\Omega v_y \sin(\beta), \tag{4}$$

which is only a second order effect.

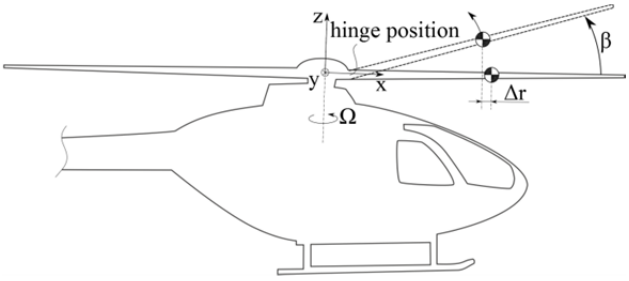

FIG 1 Schematic view of a helicopter with a flapping rigid blade

4.2.2. Generic Test Case

Since the inboard movement of the FE nodes of the blade resulting from its bending is computed in SIMPACK, the effect of the Coriolis acceleration was expected to become apparent. To investigate this, generic test cases were used. One of those cases was to excite the blade tip with a periodic force acting in flap direction with the frequency of the rotor. The aerodynamic forces were not incorporated for the test case. In FIG 2 the results for the deflection of the blade at the blade tip are shown versus the azimuth. An additional S4 calculation without the usage of the secondary mode components designated ‘S4 no SMC’ is shown in the diagrams. A good correlation can

be observed in the flap deflection z. The differences in torsional direction ϑ are because of the fact that in SIMPACK secondary mode components with a phase shift to the main component can arise, which is not possible in S4. This is discussed briefly at the end of this chapter. The mean static deflection that is apparent in all calculations originates in the propeller moment caused by the built-in twist of the blade.

In lag direction y not only the amplitude but also the frequency contents of the motion differ. The radial movement of the blade mass points towards the axis of rotation takes place when the blade is flapping upward from its horizontal position as well as during the downwards movement away from it, which is twice per flap period. Therefore, the component of the lag movement due to flapping should be twice the frequency of the flap movement in absence of a mean flap deflection. In this test case the flap deflection only has a small static value which is caused by the gravity. The expected 2/rev component can be seen in the S4 calculations. The additionally arising 1/rev component is caused by the incorporation of the secondary mode components. This can be demonstrated by comparison with the results of the S4 calculation without secondary mode components where only the 2/rev component remains. In the SIMPACK calculation only an oscillation with the same frequency as that of the flapping is visible. Hence, the movement originates solely from the secondary mode component of the first flap mode in SIMPACK.

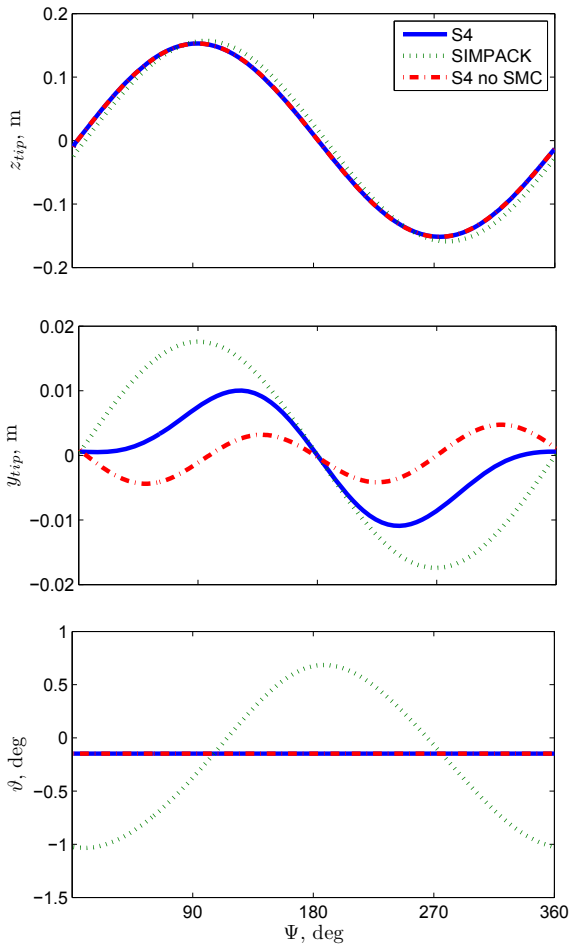

FIG 2 Tip deflections of the simplified HART II blade due to a periodic excitation in flap direction

4.2.3. Representation of Flexible Body Deformations in SIMPACK

To explain the absence of dynamic influence despite the computation of kinematics of the radial motion due to bending of the blade, the representation of flexible bodies in SIMPACK has to be given a closer look.

Within SIMPACK the motion of flexible bodies is represented by the rigid body motion of a floating frame of reference plus the deformation of the body. The deformation is dependent on mode shapes of the flexible structure and time dependent generalized coordinates $\boldsymbol{q}(t)$:

$$(5)\quad \boldsymbol{u}(\boldsymbol{R},t)=\boldsymbol{u}\big(\boldsymbol{\Phi}(\boldsymbol{R}),\boldsymbol{q}(t)\big),\quad \boldsymbol{\vartheta}(\boldsymbol{R},t)=\boldsymbol{\vartheta}\big(\boldsymbol{\Psi}(\boldsymbol{R}),\boldsymbol{q}(t)\big)$$

Hereby, $\boldsymbol{u}$ is the translational and $\boldsymbol{\vartheta}$ the rotational deformation. The translational and rotational shape functions $\boldsymbol{\Phi}$ and $\boldsymbol{\Psi}$ only depend on the position $\boldsymbol{R}$ on the elastic body [12].

Already in an early version of SIMPACK the modeling of flexible beams included quadratic expansion of nonlinear movements, as stated in [12]. This means, the deformation is dependent on a linear and quadratic term shape function multiplied with the generalized coordinates and a second order term, respectively. The corresponding formula reads as follows for a distinct direction i [12]:

$$(6)\quad u_i(\boldsymbol{R},t)=\boldsymbol{\Phi}_{Li}(\boldsymbol{R})\boldsymbol{q}(t)+\frac{1}{2}\boldsymbol{q}^T(t)\boldsymbol{\Phi}_{Qi}(\boldsymbol{R})\boldsymbol{q}(t)$$

Here, the subscript L stands for the linear and Q for the quadratic expansion mode shapes for the node at $\boldsymbol{R}$.

As this approach was applied in the calculation of all relevant matrices, the dynamic effects of tilting and bending were also included. This means that the interface for generation of the data needed to model the elastic body in SIMPACK as well as the solver of SIMPACK were able to handle the higher order formulation of all generalized mass submatrices, generalized inertia force matrices and gyroscopic matrices. In the definition of the standard input data format, the possibility of higher order formulations is given as well [13].

For the incorporation of a new preprocessor for three-dimensional (3D) beam structures a different approach was used, however. A linear approximation of the displacement field yields

$$(7)\quad \boldsymbol{u}(\boldsymbol{R},t)=\boldsymbol{\Phi}(\boldsymbol{R})\boldsymbol{q}(t)$$

and leads to much simpler matrices in the equations of motion [14]. In these equations now only linear effects are represented. The correction of the displacements for the nonlinear movement is done separately using the correlation

$$(8)\quad \boldsymbol{\Phi}_{Qi}^k=-\boldsymbol{K}_{geo}\big(\boldsymbol{F}_i^k=1\big)$$

for node k established for beam structures in [15]. Equation (8) states that the nonlinear shape function term of the deformation in direction i is equal to the negative value of the geometric stiffness matrix $\boldsymbol{K}_{geo}$ as a result of a unit load in that direction at the same node $\boldsymbol{F}_i^k$.

This means that the nonlinear effects are used in the calculation of the kinematics of points on elastic bodies but not in the equations of motion, e.g. in the matrices of gyroscopic forces. This obviously is also the case for flexible structures integrated into SIMPACK via the FlexModal interface. Thus, to enable the calculation of the

nonlinear movement of the node in SIMPACK, the static strain caused by a unit load acting on the node in that direction has to be calculated in a FEM tool like NASTRAN and the results be given to the SIMPACK converter mentioned in the introduction.

The restriction to linear deformation in SIMPACK's flexible body dynamics also entails no change in the centrifugal forces for a hingeless rotor when the blade exhibits deformations. Hence, there is no deviation between SIMPACK and S4 regarding the differential equations, unlike stated in TAB 1. In the synthesis of the rotor head forces in S4, however, the influence on the radial forces is taken into account. For an articulated rotor, the component resulting from rigid body motion will be taken into account in the differential equations in SIMPACK.

4.2.4. Solutions for Consideration of the Coriolis Forces

Two possible solutions for the incorporation of the Coriolis effect were investigated. Since the nonlinear movement of points on the blade can be measured during simulation, one could use the measured axial velocity, calculate the resulting inertial force for the blade elements and apply it onto the blade via force elements. This method did not work when applied to the model because of divergent behavior of the blades. The reason regarding this problem was not found yet. Another option would be to split up the blade in a number of individual flexible bodies and connect them via zero degree of freedom (DoF) joints. This way the nonlinear movement of every end point of the individual elements will be used as the rigid body movement of the attaching outboard element and therefore the effect will be included inherently. Results of this approach will be shown in the next chapter.

4.2.5. Phase Shift between Mode Components

The characteristics of the computed modes in S4 and SIMPACK vary in an important issue due to the different approaches used to get the eigenvalues and modes. In the S4 FE preprocessor the approach of virtual displacements is applied to the formula that describes the energy of the system. Neglecting the right hand side of the equation system this leads to a differential equation system of second order

$$(9)\quad \boldsymbol{M}\ddot{\boldsymbol{u}} + \boldsymbol{K}\boldsymbol{u} = \boldsymbol{0}$$

with symmetric mass matrix $\boldsymbol{M}$ and stiffness matrix $\boldsymbol{K}$. Applying the approach

$$(10)\quad \boldsymbol{u} = \boldsymbol{c}\, e^{\lambda t}$$

for the solution of the deflections $\boldsymbol{u}$, where the amplitude of the motion is represented by $\boldsymbol{c}$ and the change over time is characterized by λ, and substituting $\lambda^2=\Lambda$ leads to the eigenvalue problem

$$(11)\quad (\boldsymbol{M}\Lambda + \boldsymbol{K})\,\boldsymbol{c} = \boldsymbol{0}.$$

As the matrices $\boldsymbol{M}$ and $\boldsymbol{K}$ are symmetric, only negative real eigenvalues Λ are found as solution of the eigenvalue problem. This in turn also only yields real eigenvectors $\hat{\boldsymbol{c}}$. Hence, no phase shift except zero or 180° between components can be computed with this approach; the modes just give the relation of the maximum deflections. The eigenfrequencies of the system are the square root of the absolute value of the eigenvalues Λ.

In order to compute the modes of the rotating system in SIMPACK, first of all the quasi-steady equilibrium condition has to be determined. Then, the system equations are linearized around this equilibrium condition. The result is a state space system representation

$$(12)\quad \dot{\boldsymbol{x}} = \boldsymbol{A}\,\boldsymbol{x} + \boldsymbol{B}\,\boldsymbol{z}$$

with system matrix $\boldsymbol{A}$, input matrix $\boldsymbol{B}$, the vector of system states $\boldsymbol{x}$ and the input vector $\boldsymbol{z}$. After that, the eigenvalues of the system matrix are determined as solution of the free movement of the system $\dot{\boldsymbol{x}}=\boldsymbol{A}\,\boldsymbol{x}$. Due to the fact that the system matrix $\boldsymbol{A}$ is not symmetric the eigenvalues can now be complex. As a result also the eigenmodes can consist of a real and an imaginary part. Thus, the phase shift between components of the modes can have arbitrary values.

In the results of the generic test case in FIG 2 this difference in the computational approach is clearly visible in the computed torsional deflections. The first flap mode of the rotating system exhibits a phase shift of 90° between the main and the torsional component in SIMPACK. This leads to the motion in SIMPACK that is not computed with S4.

5. REFINED BLADE MODELS

As stated above, with the description of the elastic blade used up to now, the Coriolis effect is not considered. Another drawback for helicopter applications was already discussed in [10], which is the lack of the propeller moment for 1D beam representations of the flexible blade. In this chapter the attempt to overcome the limitations mentioned before will be presented using the articulated blade of the 7A model rotor.

5.1. Elastic Rotor Blade Modeling

The structural dynamics of the 7A rotor blade are modeled using a combination of FE theory and multibody dynamics. A description of the model rotor can be found in [16]. The elastic properties are defined in the FE code MSC NASTRAN which enables the definition of 1D cross-sectional blade properties (EA, EI_z, EI_y, and GJ). These beam elements are integrated into the multibody code SIMPACK using the FE interface. Three different approaches are applied for the description of the elastic rotor blade:

1) The complete rotor blade is represented by one elastic body. This is the one-body approach used up to now for the representation of the flexible blade and will be denoted "1D SIMPACK" further on.
2) The rotor blade is split into 38 elastic segments which are connected by zero DoF joints. Each 1D beam segment is integrated into SIMPACK separately. This allows for the description of each segment by a superposition of nonlinear rigid body motion plus elastic deformation. This approach is denoted hereafter as body chain or "1D SIMPACK chain".
3) In addition to the 1D model approaches, a high-fidelity 3D FE model of the 7A blade has been generated. The rotor blade model was created based on ONERA (Office national d'études et de recherches aérospatiales) /Aerospatiale reports as presented in [17]. The geometry and material properties are reconstructed. The composite of the blade is modeled

by 4-node shell elements and the blade's internal, such as spar and foam, is represented by 8-node brick elements as shown in FIG 3. The complete 3D FE model contains 74643 grid nodes. For the integration of the model into SIMPACK a condensation of the DoF is required. In total 39 master nodes along the elastic blade axis are defined. These are representing the structural blade dynamics with 234 static DoF and 30 dynamic DoF. The deformation field of the reduced 3D model is also described by the "one-body approach" in SIMPACK. The results obtained with this model are denoted "3D SIMPACK" further on.

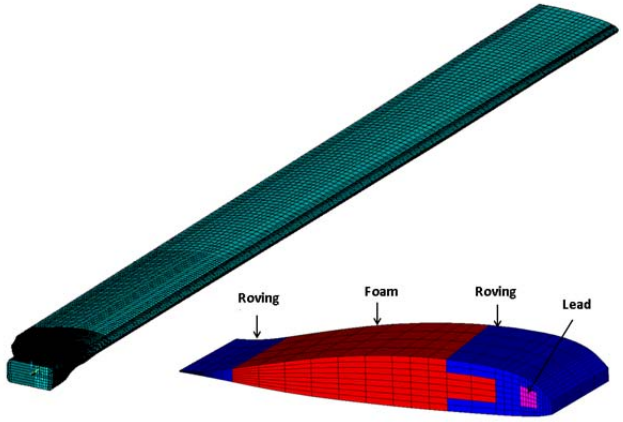

FIG 3 3D FE model of the 7A blade as shown in [17]

5.2. Structural Blade Dynamics

The Campbell diagram of the articulated 7A rotor system is given in FIG 4. Both 1D SIMPACK models, as body chain and as one-body approach, show very similar frequencies. A small difference can be identified for the first torsion frequency 1T and the fourth flap frequency 4F at nominal rotation speed Ω_{ref}. The 3D model predicts constantly higher frequencies than the 1D models for second to fifth flap mode 2F - 5F. The fourth flap frequencies of the 1D models are between the 6-7/rev rotor harmonics, whereas the 3D model predicts a frequency close to the 7/rev. The eigenfrequencies computed with the FE preprocessor of S4 correlate quite well with those of the 1D SIMPACK models except for the 1T and 4F frequencies close to Ω_{ref}. There, not only a difference in the frequencies arises but the coupling behavior is different as well. The curves of the mode frequencies crossing each other without disturbance means these modes are not coupled nearly as much as those of the other models.

The corresponding eigenmodes 1T and 4F at nominal rotation speed are shown in FIG 5 and FIG 6, respectively. Each mode comparison includes the flapwise component Φ_z, edgewise component Φ_y and torsional component Φ_ϑ. The deflections are normalized by the blade tip deflection of their respective mode's main component. The torsion mode shows similar torsional distributions for the different rotor blade models. The 1D SIMPACK model shows bigger secondary mode components Φ_z for the torsion mode 1T than the other SIMPACK models. Despite the different modeling approaches, the resulting modes are quite similar in SIMPACK, however. Larger differences are revealed comparing the SIMPACK results to those of the FE preprocessor of S4. In the upper diagram of FIG 5 it is clearly visible that there is almost no bending-torsion-coupling apparent for the torsion mode. The same holds true for the fourth flap mode 4F shown in the lower diagram of FIG 6, where the torsional secondary mode component is much smaller than that of the SIMPACK models. The mentioned deviations reflect the expected difference in coupling behavior deduced from the Campbell diagram.

One expected benefit of transferring the reduced 3D model of the blade into SIMPACK was the direct incorporation of the propeller moment. In FIG 7 the radial distribution of the torsional deformation is given for the blade rotating in vacuo with a pitch angle of 15°. The results of the 1D SIMPACK chain are obtained with additional force elements accounting for the propeller moment as introduced in [10]. The occurrence of a deflection for the SIMPACK 3D model is an indication of the propeller moment's representation, because there would be virtually no torsional deflection without propeller moment. On the other hand, the absolute value of the deflection as well as the shape of the curve differs from the results obtained with the 1D SIMPACK chain with additional force elements and the S4 calculation. The latter two show a good agreement with each other and approach what would be expected from beam theory. A difficulty in the transfer of the 3D model into SIMPACK is the definition of the superelement nodes for the representation of the dynamics. A more detailed description and investigation of the dynamics of the 3D model is given in [17]. There, it was also stated that the linear deformation field of the reduced 3D model in SIMPACK did not yield a sufficient bending-torsion deformation. Therefore, this model will not be used in the following calculations.

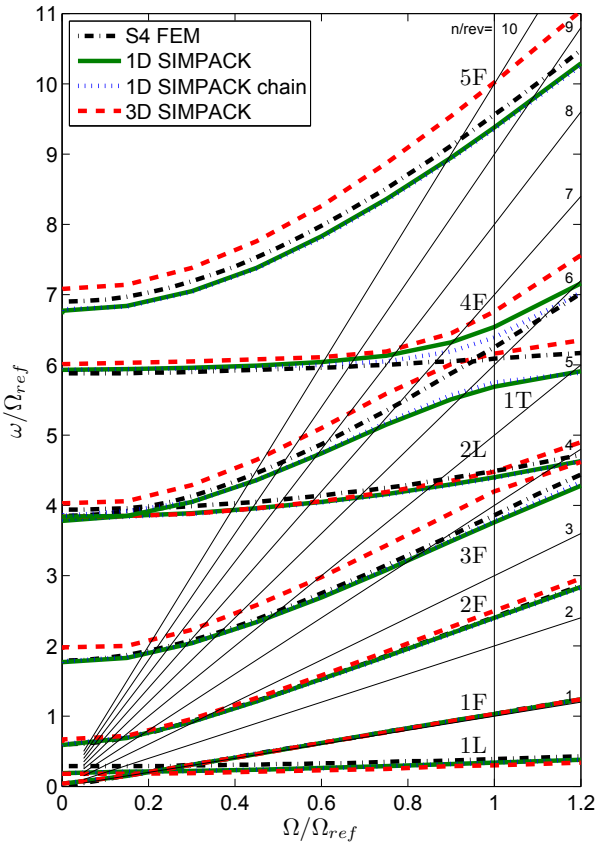

FIG 4 Campbell diagram of the articulated 7A rotor

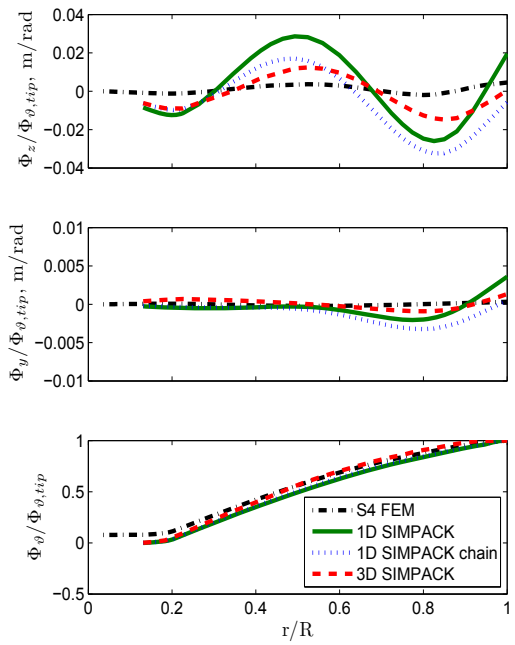

FIG 5 Comparison of the first torsion mode 1T of the 7A rotor with the different modeling approaches

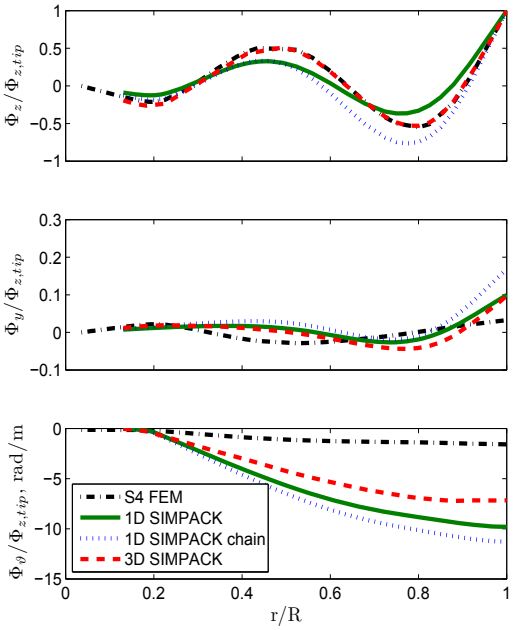

FIG 6 Comparison of the fourth flap mode 4F of the 7A rotor with the different modeling approaches

The 1D SIMPACK chain, on the other hand, is expected to correctly consider the Coriolis effect through usage of the nonlinear movement of the single bodies in the equations of motion. To prove this, again generic forces acting periodically on the rotor blade tip were used. The blade was excited in clamped configuration to capture the effects of the elastic bending of the blade only. In FIG 8 the deflections in flap, lag and torsion caused by a force acting in flap direction changing with the rotational frequency of the rotor are shown. The quite good correlation of the S4 and SIMPACK structural response in flap direction that was apparent in FIG 2 can be observed here, too.

A great difference compared to the previous results is the change of the main component of the lag motion to twice the frequency of the flap motion in the SIMPACK calculation. This proves that the Coriolis terms occur as expected. The result of the S4 calculation without secondary mode components shows that the motion due to Coriolis in SIMPACK is of the same magnitude as in S4.

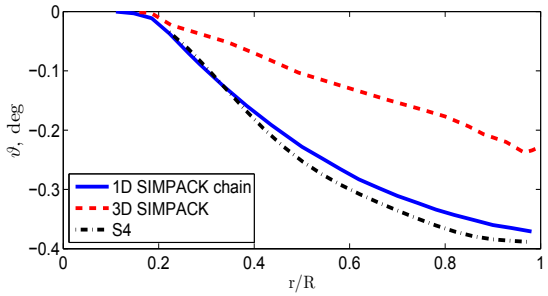

FIG 7 Torsional deformation of the different blade models for rotation in vacuo with a pitch angle of 15°

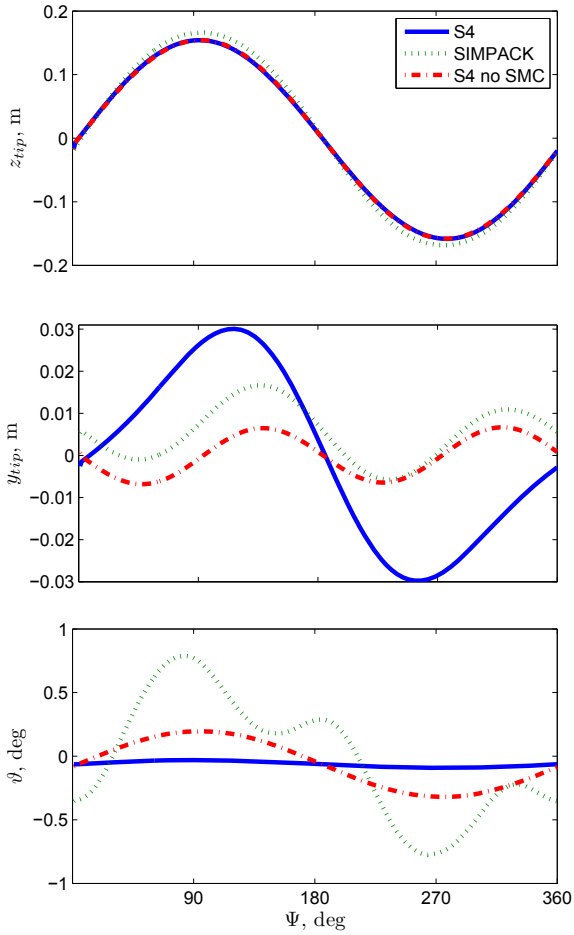

FIG 8 Tip deflections of the clamped 7A blade using a 1/rev excitation in flap direction

The secondary mode component of the flap mode yields the additional 1/rev movement in the “normal” S4 calculation and the SIMPACK calculation. Since this component is bigger in the S4 calculations the resulting

movement exhibits larger deviations. In torsional direction now a movement in the S4 calculations is observed in contrast to the results shown for the simplified HART II blade. This is because of the fact that all axis offsets of the blade are accounted for, which causes a bending-torsion coupling.

6. THE 7A ROTOR IN HIGH SPEED FORWARD FLIGHT CONDITION

The results presented in this chapter are based on the calculation of the 7A rotor performing a high speed forward flight. The experimental data were gathered in a wind tunnel test campaign that took place in 1990 in the S1 wind tunnel in Modane [16]. The rotor has four blades and the blade attachment system is of the articulated type. Some technical data and the operating conditions of the test point 312 that was used for these investigations can be found in TAB 2. In Addition to the aerodynamic coefficients shown in the table, two conditions for the trim flap angles were formulated, also known as the Modane flapping law. The conditions are that the lateral flapping angle β_s=0 and the longitudinal flapping angle β_c = - θ_s which is the longitudinal pitch control angle.

Description	Symbol	Value
Rotor radius	R	2.1 m
Geometric solidity	σ	0.0849
Prelag	ζ_p	-4°
Rotational speed	Ω	106 rad/s
Advance ratio	μ	0.401
Rotor lift coefficient	C_L/σ	0.0628
Propulsive force coefficient	C_X/σ	0.1

TAB 2 Rotor and operational condition data

Trim calculations for S4 standalone and coupled S4-SIMPACK calculations have been conducted using the collective and the longitudinal and lateral cyclic pitch control angles as well as the rotor shaft angle α_{Ro} as trim DoF. In S4, five flap modes, three lag modes and two torsion modes are considered. The induced velocities are calculated by the approach of Mangler and Squire [18]. In the SIMPACK model, due to the splitting into blade elements, a maximum of 228 modes could be considered for each blade. This leads to higher computational costs and possible numerical instabilities as a result of excitation of poorly damped high frequency modes because of the unsteady aerodynamics. Hence, the number of modes was reduced for the computations, but still a total of 504 modes were considered for the rotor.

The trim angles are shown in TAB 3. All values obtained with S4 show only a fair agreement with test conditions. In the S4-SIMPACK simulation, the lateral control angle is closer to the experimental value, whereas the Rotor shaft angle shows a greater deviation. It has to be stated here that the aerodynamic interferences with the wind tunnel walls, the rotor hub and the model support fairing were not incorporated in the investigations. For comparison, the results of the simulation of this test case using a coupling of SIMPACK and the CFD solver TAU as explained in detail in [17] are given. For the TAU-SIMPACK calculation a greater deviation of the trim values is apparent for the lateral trim angle only.

	α_{Ro}	θ_0	θ_s	θ_c
Experiment	-13.75°	14.54°	-3.7°	3.43°
S4	-11.54°	12.73°	-2.62°	0.91°
S4-SIMPACK	-10.92°	12.35°	-2.60°	1.34°
TAU-SIMPACK	-12.67°	14.45°	-3.71°	1.20°

TAB 3 Comparison of experimental and simulated trim values

In FIG 9 the lift force on the blade section at the blade tip is depicted for the different simulations together with the experimental values. Using the aerodynamics of S4 shifts the negative peak of the force to Ψ=90°. Also, the peak is much stronger in the S4 calculations although less pronounced in the coupled S4-SIMPACK simulation. This is compensated for by a higher lift coefficient throughout the bigger part of the revolution. The TAU-SIMPACK simulation shows a good agreement with the experiment regarding the phase of the negative peak, but the amplitude is smaller.

FIG 10 shows the aerodynamic pitch moment at the blade tip. The most prominent distinction between measured values and the S4 simulation is the occurrence of a dual negative peak in the latter ones. Apart from the peaks the moment is close to zero in the S4 calculations. In the experiment and the CFD result a continuously rising moment occurs apart from the negative peak. All three effects, namely the azimuthal shift of the normal force peak, the dual moment peak and the moment remaining at small values apart from the peaks were also occurring in calculations of this test case with other comprehensive codes. This was presented in [19], where the programs used were the helicopter overall simulation tool HOST and the rotorcraft comprehensive analysis system RCAS.

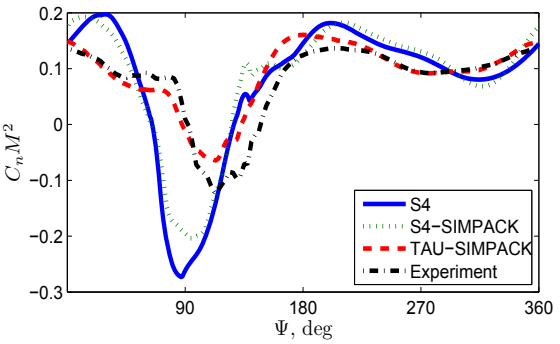

FIG 9 Section normal coefficient force at r/R=0.98

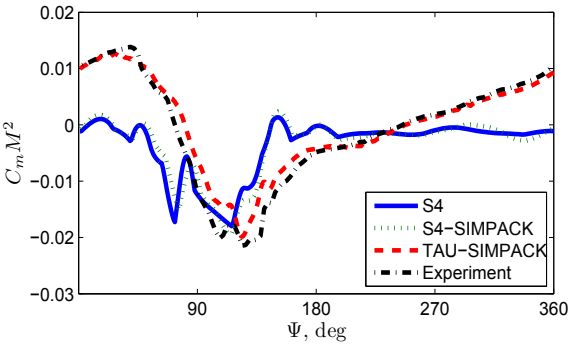

FIG 10 Section moment coefficient at r/R=0.98

The torsional deflections close to the blade tip are shown in FIG 11. The main characteristic in the experimental results is the 5/rev motion which is apparent in both calculations using the 1D beam chain of SIMPACK. The magnitude of the main peak is also captured by the S4 standalone calculations, but the 5/rev component is much smaller. Presumably resulting from the shift of the moment peaks in S4, also the torsional deformations show an azimuthal shift of the main peak to smaller values. There is also a shift between the TAU-SIMPACK result and experiment although almost no shift of the torsional moment peak has occurred there, however. The result of the coupled S4-SIMPACK calculation shows a second area of higher torsion for $270 < \Psi < 360°$. Further investigations are needed to find an explanation for this phenomenon.

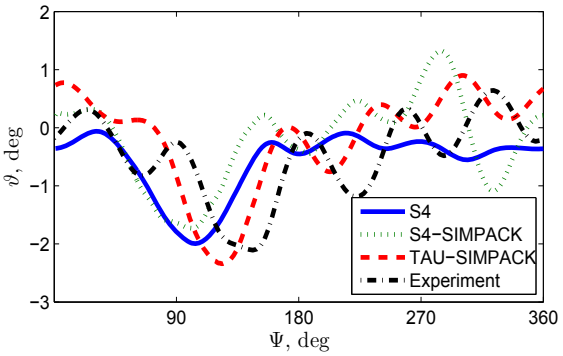

FIG 11 Elastic torsion at r/R=0.96

7. SUMMARY AND CONCLUSION

In this paper the advances in coupling of S4 with rotor models in SIMPACK were presented. Starting with dynamic excitation of a hingeless rotor model, the absence of the Coriolis effect for elastic blades in SIMPACK due to deformations was discovered. A closer investigation of the modeling of deformations in SIMPACK yielded that the nonlinear kinematics of points on an elastic body can be represented in SIMPACK whereas in the equations of motion only linear movement is considered.

A substructuring technique was employed for the 1D beam approach to integrate the Coriolis effect into the model. As a result, a much higher number of modes have to be retained in the model to correctly describe the blade modes, since they are a combination of the modes of the single blade elements. Due to the number of possible modes, the determination of the modes which have to be considered is a quite challenging task. In this area further investigations are needed. Very high frequency oscillations or unrealistic blade motion behavior were likely to occur with usage of all modes and step or impulse excitations. Another approach to reduce the number of modes needed would be to split up the blade into fewer parts. In that case, a tradeoff between computational effort and accuracy of dynamic description has to be found. Results obtained with a 3D model of the 7A blade suggest that the propeller moment is incorporated in the blade dynamics.

In the last part of the paper, results of calculations of a high speed forward flight case of the 7A model rotor were compared to experimental data obtained in a wind tunnel test campaign. The deviations in aerodynamic parameters that were found for the calculation of aerodynamics in S4 were matching those already obtained with other comprehensive codes. In the discussion of the results it was stated by the investigators that it is unlikely that comprehensive analysis results for this test case can be significantly improved. Nevertheless, accounting for the model support for example is expected to have an influence on the lateral trim angle and therefore would yield a change of overall aerodynamic behavior.

Further studies will be carried out to investigate the representation of the dynamic effects of large axis offsets and precone. Especially for hingeless rotors, where all movements of the blade relative to the hub are caused by elastic deformation, the correct incorporation of all important effects is crucial for reliable simulations.

8. REFERENCES

[1] P. Rauch, M. Gervais, P. Cranga, A. Baud, J.-F. Hirsch, A. Walter, and P. Beaumier, “Blue Edge™: The Design, Development and Testing of a New Blade Concept”, 67th Annual Forum of the American Helicopter Society, Virginia Beach, VA, May 3-5, 2011

[2] B.G. van der Wall, C. Kessler, Y. Delrieux, P. Beaumier, M. Gervais, J.-F. Hirsch, K. Pengel and P. Crozier, ”From ERATO Basic Research to the Blue Edge™ Rotor Blade”, 72th Annual Forum of the American Helicopter Society, West Palm Beach, FL, May 17-19, 2016

[3] W. Johnson, “Rotorcraft Aeromechanics Applications of a Comprehensive Analysis”, AHS International Meeting on Rotorcraft Technology and Disaster Relief, Gifu, Japan, April, 1998

[4] B. Benoit, A.-M. Dequin, W. von Grünhagen, K. Kampa, P.-M. Basset and B. Gimonet, “HOST, a General Helicopter Simulation Tool for Germany and France”, 56th Annual Forum of the American Helicopter Society, Virginia Beach, VA, May 2-4, 2000

[5] H. Saberi, M. Khoshlahjeh, R.A. Ormiston and M.J. Rutkowski, “Overview of RCAS and Application to Advanced Rotorcraft Problems”, 4th Decennial Specialist’s Conference on Aeromechanics, San Francisco, CA, Jan. 21-23, 2004

[6] G. Bir, I. Chopra and K. Nguyen, “Development of UMARC (University of Maryland Advanced Rotorcraft Code)”, 46th Annual Forum of the American Helicopter Society, Washington, D.C., May, 1990

[7] B. Glaz, P. P. Friedmann, L. Liu, D. Kumar, C.E.S. Cesnik, ”The AVINOR Aeroelastic Simulation Code and its Application to Reduced Vibration Composite Rotor Blade Design”, 50th AIAA/ASME/ASCE/AHS/ASC Structures, Structural Dynamics, and Materials Conference, Palm Springs, CA, May 4-7, 2009

[8] B.G. van der Wall, J.W. Lim, M.J. Smith, S.N. Jung, J. Bailley, J.D. Baeder and D.D. Boyd Jr., “The HART II International Workshop: an Assessment of the State-of-the-art in Comprehensive Code Prediction”, CEAS Aeronautical Journal, **4**(3), 2013, pp. 223-252

[9] J. C. Houbolt and G. W. Brooks, "Differential Equations of Motion for Combined Flapwise Bending, Chordwise Bending and Torsion of Twisted Nonuniform Rotor Blades," NACA Report TR 1346, 1958

[10] J. Hofmann, L. Krause, M. Mindt, M. Graser and S. Surrey, "Rotor Simulation and Multibody Systems: Coupling of Helicopter Aerodynamics with SIMPACK“, 63. Deutscher Luft- und Raumfahrtkongress, Augsburg, Germany, Sept. 16-18, 2014
[11] D. Gross, W. Hauger, J. Schröder, W.A. Wall, “Technische Mechanik Band 3: Kinetik“, Springer Verlag Berlin Heidelberg, 2006
[12] O. Wallrapp, “Nonlinear Deformations in Flexible Multibody Systems”, Euromech Colloquium 427, Paris, France, Sept. 24-27, 2001
[13] O. Wallrapp, “Standardization of Flexible Body Modeling in Multibody System Codes, Part I: Definition of Standard Input Data”, Mechanics of Structures and Machines, **22**(3), 1994, pp. 283-304
[14] O. Wallrapp, “Standardization and Preparation of Flexible Body Data in Multibody Formulations”, AAS/AIAA Astrodynamics Specialists Conference, Halifax, Canada, Aug. 14-17, 1995
[15] O. Wallrapp and R. Schwertassek, “Representation of Geometric Stiffening in Multibody System Simulation”, International Journal for Numerical Methods in Engineering, **32**(8), 1991, pp. 1833-1850
[16] C. Polacsek and P. Lafon, “High-Speed Impulsive Noise and Aerodynamic Results for Rectangular and Swept Rotor Blade Tip Tests in S1-Modane Wind Tunnel”, 17th European Rotorcraft Forum, Berlin, Germany, Sept. 24-27, 1991
[17] S. Surrey, B. Ortun, K.-V. Truong and F. Wienke, “Investigation of the structural blade dynamics and the aeroelastic behavior of the 7A rotor”, 72nd Annual Forum of the American Helicopter Society, West Palm Beach, FL, May 17-19, 2016
[18] K. W. Mangler and H. B. Squire, “The Induced Velocity Field of a Rotor”, ARC R&M 2642, 1950
[19] B. Ortun, M. Potsdam, H. Yeo and K.-V. Truong, “Rotor Loads Prediction on the ONERA 7A Rotor using Loose Fluid/Structure Coupling”, 72nd Annual Forum of the American Helicopter Society, West Palm Beach, FL, May 17-19, 2016